International Journal of Allied Sciences (IJAS)
Volume.14, Number 12; December-2023;
ISSN: 2836-3760 | Impact Factor: 9.83
https://zapjournals.com/Journals/index.php/Allied-Sciences
Published By: Zendo Academic Publishing

COMPUTATIONAL INSIGHTS: NUMERICAL SIMULATION AND WENO ANALYSIS OF DIRECT FORCE FEATURES

Xing Zhou Wei [1]

Article Info

Keywords: Direct Force Active Control, Precision-Guided Weapons, Lateral Jets, Aerodynamic Interference, Aircraft Control Mechanism.

Abstract

In the pursuit of precision-guided weapons, the direct force active control technology, particularly in direct gas composite, has emerged as a critical and promising avenue. This technology empowers aircraft with the ability to execute large motor and agile flights, filling the void left by conventional aerodynamic forces and boosting maneuverability and targeting accuracy. To achieve this, the utilization of thrust vectoring or lateral jets is pivotal to generate lateral forces for auxiliary control. The employment of lateral jets presents several noteworthy advantages over traditional air rudder control:

Swift control response, enhancing the capacity for kinetic energy-based target interception.

Mitigation of pneumatic heating's ablation effect on components during hypersonic flight.

Improved control efficiency in low-speed, low-density conditions when aerodynamic steering surfaces falter.

Effective lateral force provision during the final approach phase, especially when the main engine is no longer operational.

However, the intricacies of controlling lateral jets in atmospheric conditions, where the jet's interference with the aircraft's trajectory can deviate significantly from the jet thrust, necessitate a thorough exploration of the aerodynamic interference flow field. This involves simulating the interference flow field, analyzing aircraft surface pressure distribution, and understanding their responses. The establishment of a next-generation direct lateral force control model relies on this research to inform aircraft control and jet mechanism design, ultimately improving the combat effectiveness of vehicle weapon systems.

1. Introduction

The direct force active control technology of direct gas composite is an important development direction and key technology of precision-guided weapons, which provides an effective power for the aircraft to conduct large motor and agile flight [1-3]. In order to make up for the lack of aerodynamic force, enhance the mobility of the aircraft and improve the hit accuracy, it need to use thrust vector or lateral jet to produce lateral force for auxiliary

[1] Institute of Aeronautics and Astronautics, Guilin University of Aerospace Technology, Guilin, China

control. Lateral jets directly generate a lateral force, there are many advantages: (1) its control is faster than the air rudder control response, Very beneficial to the direct collision kinetic energy killing target. (2) Can avoid the ablation effect of pneumatic heating on the components under hypersonic flight conditions. (3) At low speeds and high low density, Control efficiency of the aerodynamic steering surface decreases, and the direct lateral force can play a better control role. (4) For flying vehicle weapons with rocket engines, in the near-target phase, The main engine has often stopped working, At this time, the large motor flight of the aircraft can provide sufficient lateral force through the lateral jet, Generate sufficient lateral overload or establish a larger angle of attack [3-5]
。
Generally, in outer space or extreme altitude, because the air is very thin, the force of the jet is basically the thrust of the jet; but in the atmosphere, the jet interferes strongly with the orbit of the aircraft, and the actual control force may deviate far from the jet thrust. For example, lateral jet provides lateral force, not only jet itself thrust, and because jet and bypass interference, will cause additional lateral force and pressure change, so deeply explore the control mechanism of lateral jet aerodynamic interference flow field and simulate the interference flow field, give the aircraft surface pressure distribution and its response is the basis of a new generation of direct lateral force control model, for the control of the aircraft and jet mechanism design is necessary[6,7]. Direct force control, as an active control technology, has important applications in post-launch turning and dealing against high-speed intelligent motor escape targets. The high-precision guidance and even the direct collision effect achieved by using the direct force active control technology is of great significance to improve the combat effectiveness of the vehicle weapon system[8,9].

When the vehicle adopts the direct force / aerodynamic composite control, the lateral jet of the direct force device interacts with the bullet body winding flow, forming a complex flow field structure, so that the aerodynamic force acting on the vehicle is strongly changed. The side jet interference effect is closely related to the jet parameters, the incoming flow parameters and the aircraft appearance parameters, which makes the aircraft aerodynamic characteristics show strong coupling and nonlinear characteristics, which seriously affects the composite control quality [10,11].Therefore, in the design study of introducing the direct force composite control system, the aerodynamic characteristics and the jet characteristics in the case of the direct gas composite must be fully studied and understood, in order to establish the aerodynamic model and the direct force model that can accurately describe the side jet interference effect. The interference flow field of jet and ultrasonic flow is very complicated. High-precision numerical method is used to simulate the interference flow of aircraft under different flight conditions, which can obtain relatively reasonable results, which are mostly found in previous research [12-13].From the existing calculation results, the numerical calculation methods can more accurately simulate the complex flow [14] of the jet and the vehicle winding flow interference in the atmosphere. However, in general, the previous research work is not detailed and in-depth enough, so a more detailed discussion must be conducted to provide an analysis basis for the aircraft lateral jet control.

Using high precision numerical method to simulate the interference flow of aircraft under different flight conditions. Computational format and computing grid are always very important research content and the basis of computational fluid dynamics. With the development of computational fluid mechanics, the computational format and computational grid are increasingly demanding, but also greatly promote the rapid development of computational format and computational grid. The use of higher-order numerical formats and adaptive grid techniques are two effective ways to improve numerical accuracy [15]. Based on the high-precision numerical simulation in the field, the results of direct force jets, and the interference between multiple jets.

2. Numerical Calculation Method

When the jet interacts with the ultrasonic vehicle winding flow, it not only forms complex shock systems, but also has separation and vortex motion in the flow. Therefore, the compressible N-S equations as well as high-resolution numerical methods must be simulated.

2.1. The Average N-S Equation

2.1.1. The Average N-S Equation in the Cartesian Frame

The N-S equations are universal equations describing the fluid motion of Newtonian continuum fluids, suitable for both laminar or turbulent flows. However, under the current computational conditions, it is unrealistic to solve

the N-S equation directly. For the compressible turbulence problem, if the Reynolds time-averaging method is used, the resulting time-averaging N-S equation system is too complex to model, so the time-averaging treatment adopts the proposed mass-weighted averaging method [16,17].

Suppose that the flow meets the following conditions:

a) The fluid is a Newtonian fluid;
b) The fluid is isotropic;
c) Ignoring the total physical impact;
d) There is no heat source in the flow field.

Thus, the unsteady mean N-S equations in Cartesian coordinates $O(x, y, z)$ in conserved form is:

$$\frac{\partial U}{\partial t} + \frac{\partial E}{\partial x} + \frac{\partial F}{\partial y} + \frac{\partial G}{\partial z} = \frac{\partial E_v}{\partial x} + \frac{\partial F_v}{\partial y} + \frac{\partial G_v}{\partial z} \quad (1)$$

Where U is the field variable, E, F, G are the inviscid flux, and E_v, F_v, G_v are the viscous flux. The expression of each variable is as follows:

$$U = \begin{bmatrix} \rho \\ \rho u \\ \rho v \\ \rho w \\ e \end{bmatrix} \quad E = \begin{bmatrix} \rho u \\ \rho u^2 + p \\ \rho uv \\ \rho uw \\ (e+p)u \end{bmatrix} \quad F = \begin{bmatrix} \rho v \\ \rho uv \\ \rho v^2 + p \\ \rho vw \\ (e+p)v \end{bmatrix} \quad G = \begin{bmatrix} \rho w \\ \rho uw \\ \rho vw \\ \rho w^2 + p \\ (e+p)w \end{bmatrix}$$

$$E_v = \begin{bmatrix} 0 \\ \tau_{xx} \\ \tau_{yx} \\ \tau_{zx} \\ u\tau_{xx} + v\tau_{yx} + w\tau_{zx} + q_x \end{bmatrix} \quad F_v = \begin{bmatrix} 0 \\ \tau_{xy} \\ \tau_{yy} \\ \tau_{zy} \\ u\tau_{xy} + v\tau_{yy} + w\tau_{zy} + q_y \end{bmatrix} \quad G_v = \begin{bmatrix} 0 \\ \tau_{xz} \\ \tau_{yz} \\ \tau_{zz} \\ u\tau_{xz} + v\tau_{yz} + w\tau_{zz} + q_z \end{bmatrix}$$

Here, ρ is the density, p is the pressure, e is the total energy, and u,v,w are the mass weighted average velocity components in the x,y,z directions, respectively.

The expression of viscous stress and heat transfer is:

$$\tau_{xx} = 2(\mu+\mu_t)\frac{\partial u}{\partial x} - 3(\mu+\mu_t)\left(\frac{\partial u}{\partial x} + \frac{\partial v}{\partial y} + \frac{\partial w}{\partial z}\right) - 3\rho k$$

$$\overline{\tau_{yy}} = 2(\mu+\mu_t)\frac{\partial v}{\partial y} - 2(\mu+\mu_t)\left(\frac{\partial u}{\partial x} + \frac{\partial v}{\partial y} + \frac{\partial w}{\partial z}\right) - 23\rho k$$

$$\overline{\tau_{zz}} = 2(\mu+\mu_t)\frac{\partial w}{\partial z} - 2(\mu+\mu_t)\left(\frac{\partial u}{\partial x} + \frac{\partial v}{\partial y} + \frac{\partial w}{\partial z}\right) - 2\,3\rho k \quad (2)$$

$$\tau_{xy} = \tau_{yx} = (\mu+\mu_t)\left(\frac{\partial u}{\partial y} + \frac{\partial v}{\partial x}\right)$$

$$\tau_{yz} = \tau_{zy} = (\mu+\mu_t)\left(\frac{\partial v}{\partial z} + \frac{\partial w}{\partial y}\right)$$

$$\tau_{xz} = \tau_{zx} = (\mu + \mu_t)\left(\frac{\partial u}{\partial z} + \frac{\partial w}{\partial x}\right)$$

$$q_x = \tau_{xx}u + \tau_{xy}v + \tau_{xz}w + c_p\left(\frac{\mu}{\Pr} + \frac{\mu_t}{\Pr_t}\right)\frac{\partial T}{\partial x}$$

$$q_y = \tau_{yx}u + \tau_{yy}v + \tau_{yz}w + c_p\left(\frac{\mu}{\Pr} + \frac{\mu_t}{\Pr_t}\right)\frac{\partial T}{\partial y} \quad (3)$$

$$q_z = \tau_{zx}u + \tau_{zy}v + \tau_{zz}w + c_p\left(\frac{\mu}{\Pr} + \frac{\mu_t}{\Pr_t}\right)\frac{\partial T}{\partial z}$$

In order to close the equations, the equation of state is also required. After time homogenization, the state equation is:

$$p = (\gamma - 1)\left[\rho e - \rho\frac{u^2 + v^2 + w^2}{2} - \rho k\right] \quad (4)$$

quantity. The dimensionless process is as follows:

$$x = \frac{x}{D}, y = \frac{y}{D}, z = \frac{z}{D}, t = \frac{ta_\infty}{D}, u = \frac{u}{a_\infty}, v = \frac{v}{a_\infty}, w = \frac{w}{a_\infty},$$

$$\rho = \frac{\rho}{\rho_\infty}, T = \frac{T}{T_\infty}, p = \frac{p}{\rho_\infty a_\infty^2}, \mu = \frac{\mu}{\mu_\infty} \quad (5)$$

Where the subscript "∞" indicates free flow, a is the sound velocity, and D is the diameter of the aircraft.
For simplicity, the superscript "-" is omitted, and the dimensionless equations are as follows:

$$\frac{\partial U}{\partial t} + \frac{\partial E}{\partial x} + \frac{\partial F}{\partial y} + \frac{\partial G}{\partial z} = \frac{1}{\mathrm{Re}_D}\left(\frac{\partial E_v}{\partial x} + \frac{\partial F_v}{\partial y} + \frac{\partial G_v}{\partial z}\right) \quad (6)$$

The Reynolds number

$$\mathrm{Re}D = \frac{\rho_\infty a_\infty D}{\mu_\infty} \quad (7)$$

Mainly depends on the flight altitude of the aircraft.

2.1.3. Average N-S Equations in General Curvilinear Coordinate System

When using the difference method to solve the N-S equations, if it is discretized directly in the rectangular coordinate system, the boundary conditions need to be interpolated for approximate treatment, which inevitably leads to boundary error and reduces the accuracy of numerical solution. In addition, in order to ensure the numerical resolution of some key areas, local grid treatment is required. Therefore, when simulating the flow of complex geometric shapes, in order to accurately deal with the complex boundary conditions, a curvilinear coordinate system suitable for the boundary of the physical solution domain is introduced. The coordinate plane in this coordinate system coincides with the boundary of the physical solution domain, which is called the body fitted coordinate system, and then transformed to the calculation domain through coordinates. The calculation grid in the physical domain is curve or surface, while in the calculation domain it is straight line or plane.
Let the spatial coordinate system($\xi\eta\zeta$, ,) change with time t, and the new time coordinateτ is simply equal to the original time coordinate t, that is

$$\begin{aligned} \xi &= \xi(x, y, z, t) \quad \eta = \eta(x, y, z, t) \\ \zeta &= \zeta(x, y, z, t) \quad \tau = t \end{aligned} \quad (8)$$

Generally, the analytical formula of the above transformation is not known, but the numerical relationship between them is known, that is, the x, y, z coordinates of grid points are known, and the transformation amount of each coordinate can be calculated through finite difference:

$\xi_x = J(y_\eta z_\zeta - z_\eta y_\zeta)$, $\xi_y = J(z_\eta x_\zeta - x_\eta z_\zeta)$, $\xi_z = J(x_\eta y_\zeta - y_\eta x_\zeta)$, $\eta_x = J(z_\xi y_\zeta - y_\xi z_\zeta)$, $\eta_y = J(x_\xi z_\zeta - z_\xi x_\zeta)$, $\eta_z = J(y_\xi x_\zeta - x_\xi y_\zeta)$, (9)
$\zeta_x = J(y_\xi z_\eta - z_\xi y_\eta)$, $\zeta_y = J(z_\xi x_\eta - x_\xi z_\eta)$, $\zeta_z = J(x_\xi y_\eta - y_\xi x_\eta)$,

$$\xi_t = -x_\tau \xi_x - y_\tau \xi_y - z_\tau \xi_z$$
$$\eta_t = -x_\tau \eta_x - y_\tau \eta_y - z_\tau \eta_z \quad \zeta_t = -x_\tau \zeta_x - y_\tau \zeta_y - z_\tau \zeta_z$$
$$J^{-1} = \begin{vmatrix} \xi_x & \xi_y & \xi_z \\ x_\xi & x_\eta & x_\zeta \\ \eta_x & \eta_y & \eta_z \\ y_\xi & y_\eta & y_\zeta \\ \zeta_x & \zeta_y & \zeta_z \\ z_\xi & z_\eta & z_\zeta \end{vmatrix} \quad (10)$$

J is the transformed Jacobian determinant.
Therefore, in the body fitted coordinate system $O(\xi\eta\zeta, ,)$, the conservation form of the average NS equations is:

$$\partial \hat{Q} + \partial \hat{E} + \partial \hat{F} + \partial \hat{G} = \mathrm{Re}^{-1}\left(\partial \hat{E}_v + \partial \hat{F}_v + \partial \hat{G}_v\right) \quad (11)$$
$$\partial\tau \quad \partial\xi \quad \partial\eta \quad \partial\zeta \quad \partial\xi \quad \partial\eta \quad \partial\zeta$$

while

$$\hat{Q} = J^{-1}\begin{bmatrix} \rho \\ \rho u \\ \rho v \\ \rho w \\ e \end{bmatrix} \quad \hat{E} = J^{-1}\begin{bmatrix} \rho U \\ \rho u U + \xi_x p \\ \rho v U + \xi_y p \\ \rho w U + \xi_z p \\ (e + pU) - \xi_t p \end{bmatrix} \quad \hat{F} = J^{-1}\begin{bmatrix} \rho V \\ \rho u V + \eta_x p \\ \rho v V + \eta_y p \\ \rho w V + \eta_z p \\ (e + pV) - \eta_t p \end{bmatrix} \quad \hat{G} = J^{-1}\begin{bmatrix} \rho W \\ \rho u W + \zeta_x p \\ \rho v W + \zeta_y p \\ \rho w W + \zeta_z p \\ (e + pW) - \zeta_t p \end{bmatrix}$$

The inverter speeds U, V, W are respectively

$$U = \xi_t + \xi_x u + \xi_y v + \xi_z w$$
$$V = \eta_t + \eta_x u + \eta_y v + \eta_z w$$
$$W = \zeta_t + \zeta_x u + \zeta_y v + \zeta_z w$$

The sticky term can be written in the following form:

$$\hat{E}_v = J^{-1}(\xi_x E_v + \xi_y F_v + \xi_z G_v) = \begin{bmatrix} 0 \\ \xi_x \tau_{xx} + \xi_y \tau_{xy} + \xi_z \tau_{xz} \\ \xi_x \tau_{yx} + \xi_y \tau_{yy} + \xi_z \tau_{yz} \\ \xi_x \tau_{zx} + \xi_y \tau_{zy} + \xi_z \tau_{zz} \\ \xi_x q_x + \xi_y q_y + \xi_z q_z \end{bmatrix}$$

$$\hat{F}_v = J^{-1}(\eta_x E_v + \eta_y F_v + \eta_z G_v) = \begin{bmatrix} 0 \\ \eta_x \tau_{xx} + \eta_y \tau_{xy} + \eta_z \tau_{xz} \\ \eta_x \tau_{yx} + \eta_y \tau_{yy} + \eta_z \tau_{yz} \\ \eta_x \tau_{zx} + \eta_y \tau_{zy} + \eta_z \tau_{zz} \\ \eta_x q_x + \eta_y q_y + \eta_z q_z \end{bmatrix}$$

$$\hat{G}_v = J^{-1}(\zeta_x E_v + \zeta_y F_v + \zeta_z G_v) = \begin{bmatrix} 0 \\ \zeta_x \tau_{xx} + \zeta_y \tau_{xy} + \zeta_z \tau_{xz} \\ \zeta_x \tau_{yx} + \zeta_y \tau_{yy} + \zeta_z \tau_{yz} \\ \zeta_x \tau_{zx} + \zeta_y \tau_{zy} + \zeta_z \tau_{zz} \\ \zeta_x q_x + \zeta_y q_y + \zeta_z q_z \end{bmatrix}$$

2.2. Turbulence Model

The turbulence model adopts the low Reynolds number k–ε model. In the model k–ε , two transport equations including turbulent kinetic energy k and its dissipation rateεare included. The eddy viscosity coefficientμ_t is defined by these two equations, and the Reynolds stress is related to the eddy viscosity. According to Boussinesq's hypothesis, Reynolds stress tensor is expressed as follows:

$$-\rho\overline{u_i''u_j''} = \mu_t S_{ij} - \frac{2}{3}\rho\delta k_{ij} \quad (12)$$

$$S_{ij} = \frac{\partial \tilde{u}_i}{\partial x_j} + \frac{\partial \tilde{u}_j}{\partial x_i} - \frac{2}{3}\frac{\partial \tilde{u}_k}{\partial x_k}\delta_{ij} \quad (13)$$

$$k = \frac{1}{2}C_\mu^2 = 0.09 \quad (14)$$

$$\mu_t = C_\mu f_\mu \rho \frac{k^2}{\varepsilon},$$

Where, μ_t is the eddy viscosity coefficient, $\tilde{u}_i$, u_i'' are the average value and pulsation value respectively.

Therefore, the transport equation can be modeled as k , ε:

$$\frac{D(\rho k)}{Dt} = (pro.)_k + (dif.)_k + (dis.)_k \quad (15)$$

$$\frac{D(\rho\varepsilon)}{Dt} = (pro.)_\varepsilon + (dif.)_\varepsilon + (dis.)_\varepsilon \quad (16)$$

The modeling of each item is as follows:

$$(pro.)_k = \left[\mu_t S_{ij} - \frac{2}{3}\rho\delta k_{ij}\right]\frac{\partial \tilde{u}_j}{\partial x_i}$$

$$(dif.)_k = \frac{\partial}{\partial x}\left[\left(\mu + \frac{\sigma\mu_{kt}}{\partial k_i}\right)\frac{\partial k}{\partial x}\right]$$

$$(dis.)_k = \rho\varepsilon$$

$$(pro.)_\varepsilon = C_{\varepsilon 1} f_1 (pro.)_k \frac{\varepsilon}{k}$$

$$(dif.)_\varepsilon = \frac{\partial}{\partial x}\left[\left(\mu + \frac{\sigma\mu_{\varepsilon t}}{\partial \varepsilon_i}\right)\frac{\partial \varepsilon}{\partial x}\right]$$

$$(dis.)_\varepsilon = C_{\varepsilon 2} f_2 (dis.)_k \frac{\varepsilon}{k}$$

$C_{\varepsilon 1}=1.44, C_{\varepsilon 2}=1.92$, $\sigma_k=1.0$, $\sigma_\varepsilon=1.3$

In the above formula, f_μ, f_1 , f_2 is a modular function reflecting the effect of low Reynolds number, which is specifically expressed as:

$$f_\mu = [1-\exp(-0.0165R_y)]^2(1+20.5/R_t) \quad (17)$$

$$f1 = 1+(0.05/f\mu)^3 \quad (18)$$

$$f2 = 1-\exp(-R_t^2) \quad (19)$$

Where, $R_t=\rho k^2/\mu\varepsilon$, $R_y=\rho k y\sqrt{\mu}$ /

2.3. WENO Scheme

ENO scheme is a series of methods based on Godunov scheme. Compared with TVD scheme, it can still maintain accuracy at the discontinuity and avoid the smoothing of inherent physical oscillation by the dissipation

introduced by TVD scheme to ensure the minimum total variation. However, the polynomial construction process of ENO format is complex, and the selection of interpolation template needs a lot of logical judgment, which hinders the improvement of calculation speed. In addition, ENO format does not make full use of the information of all nodes, resulting in a certain waste. Based on the above reasons, an improved form of ENO format was proposed, which is called weighted ENO format (WENO). This improved form not only eliminates the cumbersome shortcomings of ENO, but also improves the accuracy. The WENO method is illustrated by a one-dimensional scalar system. For equation

$u_t + f(u)_x = 0$ (20)

If the space is discretized evenly, remember $x_j = j\Delta x$. Then the spatial difference in x_j can be expressed as

$$L = \frac{1}{\Delta x}\left(\tilde{f}_{j+1/2} - \tilde{f}_{j-1/2}\right) \quad (21)$$

Where $\tilde{f}_{j+1/2}$ and $\tilde{f}_{j+1/2}$ are numerical fluxes. And if the sum $\tilde{f}_{j+1/2}$ is the positive $\tilde{f}^{+}_{j+1/2}$ and negative $\tilde{f}^{-}_{j+1/2}$ flux, then there is

$$\tilde{f}_{j+1/2} = \tilde{f}^{+}_{j+1/2} + \tilde{f}^{-}_{j+1/2} \quad (22)$$

The form of numerical flux $f_{j+1/2}$ is given below, which $f_{j+1/2}$ can be written symmetrically.

$$\tilde{f}^{+}_{j+1/2} = \frac{2}{6}f_{j-2} - \frac{7}{6}f_{j-1} + \frac{11}{6}f_j + \omega_0\left(\frac{1}{3}f_{j-2} - \frac{5}{6}f_{j-1} + \frac{1}{2}f_j\right) + \omega_1\left(-\frac{1}{6}f_{j-1} + \frac{5}{6}f_j + \frac{1}{3}f_{j+1}\right) + \omega_2\left(\frac{1}{3}f_j + \frac{5}{6}f_{j+1} - \frac{1}{6}f_{j+2}\right) \quad (23)$$

Among them

$$\omega_k = \frac{\alpha_k}{\alpha_0 + \alpha_1 + \alpha_2}, \; k = 0,1,2 \quad (24)$$

$$\alpha_0^{+} = \frac{1}{10}\left(\varepsilon + IS_0^{+}\right)^{-2}, \; \alpha_1^{+} = \frac{6}{10}\left(\varepsilon + IS_1^{+}\right)^{-2} \; \alpha_2^{+} = \frac{3}{10}\left(\varepsilon + IS_2^{+}\right)^{-2}$$

$\varepsilon$is a small amount, and

$$IS_0^{+} = \frac{13}{12}\left(f_{j-2}^{+} - 2f_{j-1}^{+} + f_j^{+}\right)^2 + \frac{1}{4}\left(f_{j-2}^{+} - 4f_{j-1}^{+} + 3f_j^{+}\right)^2$$

$$IS_1^{+} = \frac{13}{12}\left(f_{j-1}^{+} - 2f_j^{+} + f_{j+1}^{+}\right)^2 + \frac{1}{4}\left(f_{j-1}^{+} - f_{j+1}^{+}\right)^2 \quad (25)$$

$$IS_2^{+} = \frac{13}{12}\left(f_j^{+} - 2f_{j+1}^{+} + f_{j+2}^{+}\right)^2 + \frac{1}{4}\left(3f_j^{+} - 4f_{j+1}^{+} + f_{j+2}^{+}\right)^2$$

The above formula is the smoothness measure of the interpolation template. By measuring the smoothness of each interpolation template, its weight coefficient is given, and then the interpolation polynomial of numerical flux is formed.

2.4. Time Dispersion

The time difference adopts the Runge-Kutta method in the form of third-order TVD . For partial differential equations

$$\frac{du}{dt} = L(u), \text{where } L(u) \text{ is the spatial differential operator} \quad (26)$$

The Runge-Kutta scheme with third-order accuracy is

$$u^{(1)} = u^{n} + \Delta t L(u^{n}) \quad u^{(2)} = \frac{3}{4}u^{n} + \frac{1}{4}u^{(1)} + \frac{1}{4}\Delta t L(u^{(1)}) \qquad (27)$$

$$u^{n+1} = \frac{1}{3}u^{n} + \frac{2}{3}u^{(2)} + \frac{2}{3}\Delta t L(u^{(2)})$$

3. Grid Generation

Grid generation was algebraic methods. First, give the grid distribution on the boundary, and then select the appropriate interpolation function to generate the middle grid through the corresponding boundary point interpolation.

Let node A, and B be the two corresponding nodes on the boundary, and take the polynomial interpolation function of the A to B grid line as

$$r = a_0 + a_1\xi + a_2\xi^2 + a_3\xi^3 \qquad (28)$$

Among them, r is the node position vector, a_0, a_1, a_2, a_3 is the parameter to be determined.

Letξ=0 ,then $r = r_A$,Letξ=1,then $r_A = r_B$,substitute into formula (28)

$$a_0 = r_A \quad a_0 \quad a_1 + a_2 + a_3 + r_B \qquad (29)$$

Seek the derivative for the formula (28)

$$\frac{\partial r}{\partial \xi} = a_1 + 2a_2\xi + 3a_3\xi^2 \qquad (30)$$

According to the geometric meaning of the derivative, $\frac{\partial r}{\partial \xi}$ is the tangent direction on the grid line AB, Letξ=0 ,then $\frac{\partial r}{\partial \xi} = n_A$,Letξ=1, then $\frac{\partial r}{\partial \xi} = n_B$,here n_A , n_B is the given value.

$$a_1 = n_A \quad a_1 \quad 2a_2 \quad 3a_3 \quad n_B = \qquad (31)$$

Solve the algebraic equations (29) ~ (31)

$$a0 = rA \quad a1 = nA \quad a2 \quad 3(=rB \quad rA) - (n - B \quad 2n + A)$$

$$a3 = nB + nA - 2(rB - rA) \qquad (32)$$

In this way, $\xi = i/N$,（i=0,1,…,N）, N is the number of nodes, and the grid distribution between A and B can be obtained. When n_A , n_B is the normal direction of the boundary on node A and B, the grid line is orthogonal to the boundary at point A and B. Moreover, the density of the grid near points A and B can be controlled by the size ofn_A, n_B the mode n_A , n_B ,The grid n_A near point A is dense and sparse when n_A large.

For the interference flow using the N-S equation, not only to encrypt the grid near the material surface, but also to encrypt the grid near the jet because the main characteristics of the flow are concentrated near the jet.

The aircraft is generally an elongated body, and the mechanism study is usually used to calculate the outflow, and the flow field calculation with the actual wing / rudder shape. The spin shape is used to calculate the upper and lower jets (allowing the angle of attack), because only the angle of attack changes, so the flow is symmetrical, can only calculate the half, and because regardless of the wing and rudder surface, the number of peripheral grids can be relatively less. Because of the presence of the wing, the grid encryption needs to be performed near the surface of the wing. In addition, the jet is located between the wing, so the grid encryption process is also required in the location of the jet. The number of grids calculated by the flow field is125×31×50 (axial / peripheral / vertical wall direction), and the grid is encrypted locally in the jet, as shown in Figure 1.

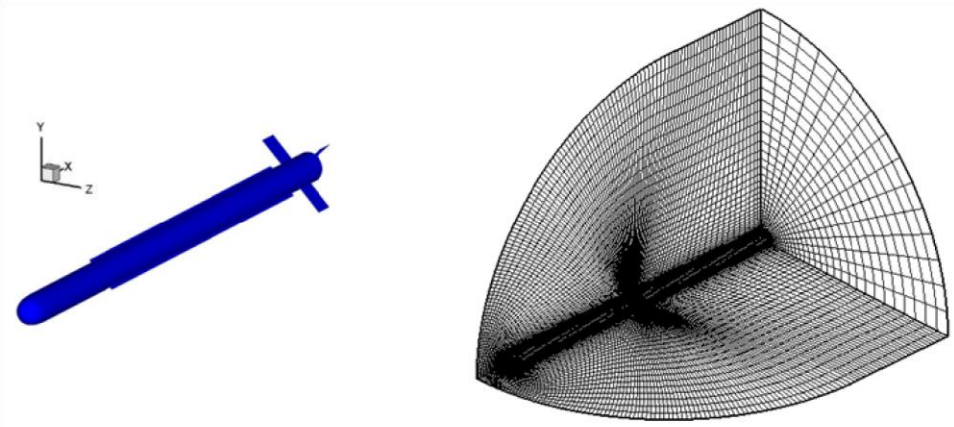

Figure 1: Shape of spin body and grid setting of aircraft

4. Initial field and boundary conditions

4.1. Initial Field

In principle, the calculation of steady flow field does not depend on the setting of initial field, but the initial field will affect the convergence process. In the calculation process, the uniform flow is taken as the initial field. Since the flow state is dimensionless in the calculation, the uniform initial field is given as follows:

$$\rho_i = 1 = \rho\infty \quad (33)$$

$$vi = a\infty\infty \; M=\infty \; V\infty\infty$$

$$pi = 2 = \rho\infty a\infty \gamma$$

$$u^2 + v^2 + w^2$$

The initial energy e can pass through the equation of state $p=(\gamma-1)e-2$, in the above formula, M is the Mach number.

4.2. Boundary Conditions

The boundary conditions include object surface boundary, symmetric boundary (including geometric symmetry axis), far field incoming flow boundary, outlet boundary, and jet flow boundary for jet flow calculation. In fact, in order to describe the flow interacting with the jet and the flow around it more closely, the internal flow field of the jet engine and the external mixed flow field should be coupled to solve the problem, but this will greatly increase the complexity and solving time of the solution, such as the need to partition calculation, and solve the problem of grid nesting. In addition, when discussing jet response, we should also establish a jet start-up model to study the impact of jet start-up process.

Because the size of the jet outlet is relatively small, only a few hundred square millimeters in the current design state, and the boundary size is far smaller than the scale of the calculation area, the flow at the jet outlet can be approximately considered to be uniform, and the jet boundary is given by onedimensional isentropic flow analysis. This simplification can grasp the main contradiction and reflect the main problems, which is reasonable.

4.2.1. The Surface Boundary

The viscous fluid meets the condition of no slip on the object surface, that is, the velocity on the object surface is zero:

$$V_w = 0 \quad (34)$$

The pressure perpendicular to the direction of the object plane adopts zero gradient condition:

$$\frac{\partial p}{\partial \zeta} = 0 \quad (35)$$

4.2.2. Symmetric Boundary

Symmetric boundary exists in symmetric flow, then only half of the flow can be calculated, and the symmetrical surface is taken as the symmetric boundary. On the plane of symmetry $\eta=0$, the following relation holds:

$$v=0,\ \frac{\partial(\rho,p,u,w)}{\partial\eta}=0 \qquad (36)$$

That is, the velocity perpendicular to the plane of symmetry is zero, and the gradient of density, pressure and velocity components perpendicular to the plane of symmetry is zero.

In the calculation, the cross sections of the symmetric surfaces j=1 and j=NJ can be expressed by second-order unilateral difference:

$$(\rho,p,u,w)_{j=1}=\frac{4(\rho,p,u,w)^{j=2}-(\rho,p,u,w)^{j=3}}{3} \qquad (37)$$

Because the O-C grid is generated, there is a geometric axis of symmetry in the warhead, where $\xi=0$ (I=1). The Jacobian determinant of the coordinate variation at the axis is singular, so special treatment must be made for the axis boundary. Here, a very simple method is adopted, that is, the physical quantity at the axis is obtained by interpolation of the average value of the surrounding physical quantities, which can be either first-order interpolation or second-order interpolation. Practice shows that, usually take the first order of interpolation:

$$(\rho,p,u,w)_{i=1}=(\rho,p,u,w)_{i=2} \qquad (38)$$

4.2.3. The Far Field Boundary

For incoming flow boundary, flow parameter is set as free incoming flow value, i.e:

$$(\rho,u,v,w,e)_{in}=(\rho,u,v,w,e)_{\infty} \qquad (39)$$

4.2.4. Outlet boundary

The outflow boundary is a fully developed boundary, all physical quantities are linear extrapolation,

$$(\rho,u,v,w,e)_{i\max}=2(\rho,u,v,w,e)_{i\max-1}-(\rho,u,v,w,e)_{i\max-2} \qquad (40)$$

4.2.5. Jet boundary

As mentioned above, jet flow is given in the form of boundary conditions. Since the spatial scale of jet flow relative to the overall flow is very small, it can be approximately calculated by one-dimensional isentropic flow method.

According to the aircraft control, the thrust of the jet should produce an acceleration of about 8g, for example. Considering the mass m=70kg of the aircraft in the passive flight section, the thrust of the jet flow

$$F_{jet}=ma=70\times 8g\approx 5500N \qquad (41)$$

Here, it is assumed that the amplification factor of jet thrust is 1, that is, the thrust of jet engine is equal to 5500N.For solid engines, the flow parameters of each section of the engine nozzle can be determined after the thrust requirements are given and the combustor pressure and propellant are selected. Take the Russia 9M96E2 as an example, its lateral jet control engine, the corresponding combustion chamber pressure of the solid engine is:

$$P_c=14MPa \qquad (42)$$

According to the formula for one-dimensional isentropic flow:

$$\frac{T_0}{T}=1+\frac{\gamma-1}{2}M^2=1+\frac{\gamma-1}{2}M^2=\frac{\rho_0}{\rho}=\left(1+\frac{\gamma-1}{2}M^2\right)^{\frac{1}{\gamma-1}}=\frac{A}{At}\left(\frac{2}{\gamma+1}\left(1+\frac{\gamma-1}{2}M^2\right)\right)^{\frac{\gamma+1}{2(\gamma-1)}} \qquad (43)$$

and

$$At=\frac{mc^*}{Pc},\ \rho t=\frac{m}{At},\ F_{vac}=mve+p_eA_e \qquad (44)$$

After the total pressure, flow rate, characteristic velocity and specific heat ratio of gas are given, flow parameters and thrust force at any section of nozzle can be determined. The jet outlet section is specified by the outlet Mach number。So in this formula up here, A represents the nozzle cross-sectional area, $^{m}\square$ is the flow rate, c* is the characteristic velocity, a is the speed of sound, M is the Mach number, F is the thrust; subscript "0" indicates stagnation parameters, subscript "t" indicates nozzle throat section, subscript "e" indicates outlet section, and "vac" indicates vacuum.

Flow parameters are given according to height according to international standard atmosphere table. After selecting some parameters of hydroxybutyrate propellant and calculating the parameters of jet outlet, the dimensionless jet boundary value needed in the calculation can be obtained.

The jet boundary parameters obtained for single jet flow, and for double jet flow, because the chamber pressure of solid engine is known, can be simplified as:

1

$$\overline{p} = \square\square\square \quad {}^{A}A\,{}^{b}t\,a\rho_b c^{*}\square_{\square}\,{}^{\square}\square^{\,1-n} \qquad (45)$$

It is assumed that a propellant with a pressure index of 0 is taken, then the chamber pressure is inversely proportional to the throat area for a given jet mechanism design. With two jets open, the throat area is twice as large, so the chamber pressure is reduced by half.

5. Calculation Results and Analysis

5.1. Upper and Lower Jet Flow Conditions

Take the flight altitude of 6km and the speed Ma=2 as the flight condition. It is assumed that the chamber pressure is 14MPa for single jet flow and 7MPa for opposite double jet flow. When the Mach number at the jet outlet is Ma=1.0, the boundary conditions of single and double jets are shown in Table 1:

Table 1: Boundary conditions for single and double jets

	$\overline{\rho}$	$\overline{\rho v}$	p	Thrust (N)	
Single jet	14.054		44.68	120.376	5486.6
Double jet	7.027	22.34	60.188	2735.8	

In the case of the opposite jet flow, it is obvious that the flow is symmetric under the condition of zero angle of attack, and the jet flow on both sides of the aircraft can achieve the balance of the lateral force. However, the jet flow on both sides may not achieve the balance under the condition of the angle of attack. Therefore, the case that the angle of attack is 10 degrees (jet flow is upper and lower side) is calculated. As the flow field is symmetrical, a half field is calculated, and the number of grids is 125×31×50 (along the axial direction, circumferential direction and perpendicular to the projectile body direction respectively).

Figures 2, 3 and 4 respectively show the Mach number, pressure and density distribution under the condition of upstream and downstream opposable jet flow. Obviously, the effect of angle of attack is very obvious, and jet flow on the windward side is blown towards the projectile by incoming flow. As can be seen from the Mach number distribution in Figure 2, the barrel shaped shock wave formed by the jet is obviously tilted on the windward side of the projectile body, and the shock wave on the windward side is slightly stronger, while the low-pressure region downstream of the jet is larger (See Figure 3). It follows that the asymmetry of the jet stream is responsible for the downward force.

Figure 5 shows the change of the pressure iso-surface under the condition of 10 degrees angle of attack, from which the interference and asymmetry of the two jets can be clearly seen. The low-pressurearea bends to the windward side, resulting in the effective force of the leeward jet is greater than that of the windward jet.

Table 2 compares the stress of the projectile body when there is no jet flow and when there is upsidedown opposite jet flow. The asymmetry of jet flow does not have much effect on the axial force, but it is obvious that their combined action produces a downward resultant force of 3729-2381 = 1348N.

Table 2: Stress of projectile body without jet flow and opposite jet flow

	Fx (N)	Fy (N)
No flow	0.2625830E+04	0.3729046E+04
The lateral jet flow	0.2659668E+04	0.2381162E+04

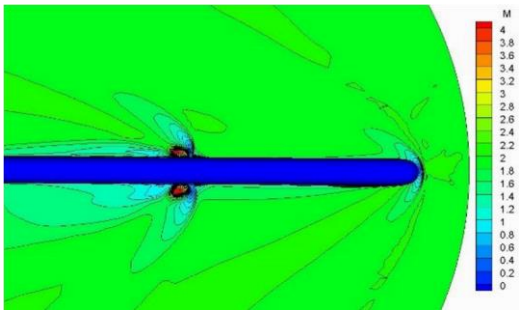

Figure 2: M distribution on the plane of symmetry

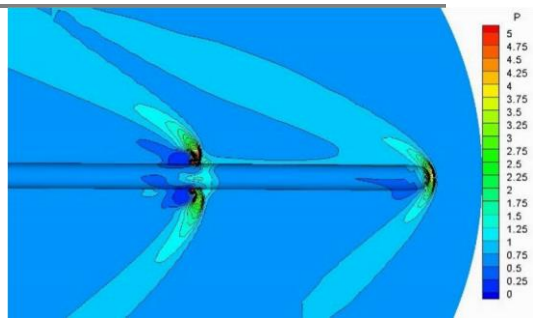

Figure 3: P distribution on the plane of symmetry

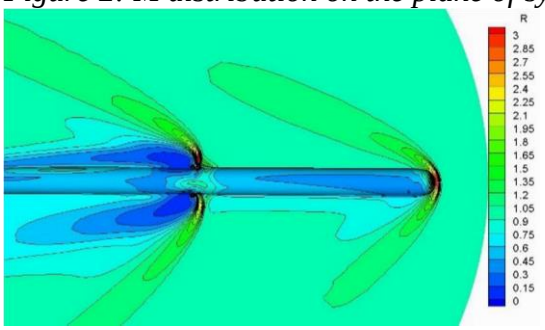

Figure 4: Density distribution on symmetry plane

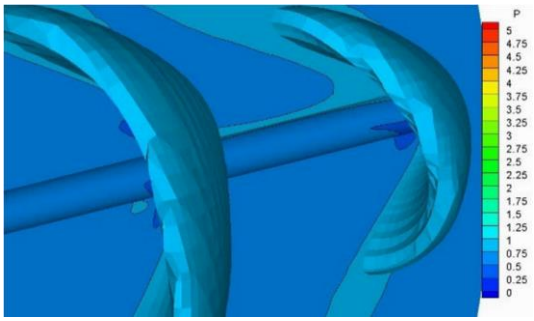

Figure 5: Isometric pressure changes

5.2. Right Angle Jet Flow Condition

Table 3 shows the stress of the projectile body under the condition of right-angle jet flow. In the case of single jet flow, the amplification factor under the same conditions is calculated to be about 0.8, but in the case of double jet flow, it can be seen that the amplification factor of jet flow is 1.12. Obviously, this difference is very large and must be taken into account in practical application. Analyzing the reason, it should be caused by the interference between the two jets.

Table 3: Stress of projectile body under right-angle jet flow condition

	Fy (N)	Resultant force
Single jet thrust	-2735.8	-3869.0
Latera lforce calculation value	-3065.8	-4335.7
Amplification factor	1.12	

Figure 6 shows the change of pressure on the cross section near the axial jet of a right-angled twin jet, from which the interference between jets can be seen.

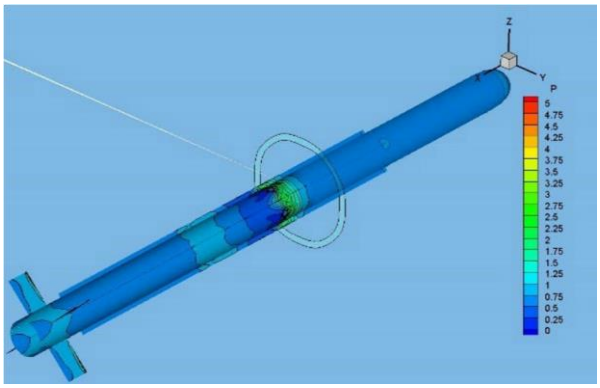

Figure 6: Pressure distribution in axial cross section of projectile body(α=0)

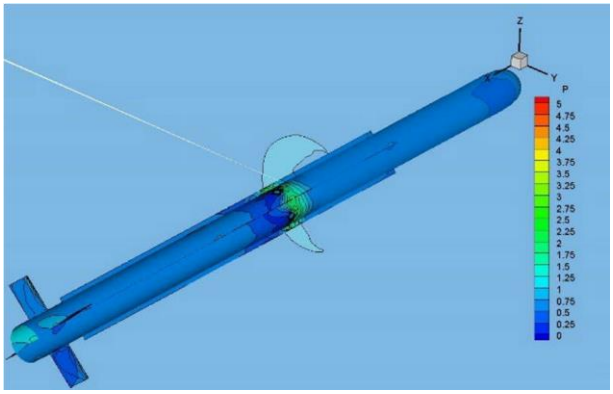

Figure 7: Pressure distribution in axial cross section of projectile body(α=10)

Figure 7 shows the pressure distribution along axial cross sections at 10-degree angle of attack, which can be compared with Figure 6 at 0-degree angle of attack (the positions of all sections are the same). Also, we find that the high-pressure area on the leeward side is stronger.

6. Conclusion

Based on the lateral jet flow and vehicle flow around more interference flow field for research object, using the method of three order WENO, through the grid generation and initial and boundary conditions are set, the direct power flow calculation, analyzed the aircraft under the typical high double workflow, and the different flight conditions or flight condition on the interaction between jets, etc. The main conclusions are as follows:

(1) Due to the asymmetry of the flow field, the force of the opposite jet flow under the condition of the Angle of attack cannot be offset. The additional force on the windward side of the projectile caused by interference is smaller than that on the leeward side.

(2) Under the action of two jets at right angles, the interference between the two jets will enhance the effect of the jet, and the equivalent amplification factor of the single jet increases.

(3) Because of the mutual interference between multiple jets, for the aircraft controlled by lateral jets, in the process of control system design, the force of the aircraft must be considered comprehensively according to the specific flight conditions, and the results of single jet cannot be simply extrapolated.

Acknowledgements

This work was financially supported by the National Natural Science Foundation of China. The project number is 61966010. Thanks for the help and support of the National Natural Science Foundation of China.

References

Fan, H. T. (2011) Characteristics and Key Technologies of the Fifth Generation Air-to-air Missile. Aeronautical science & Technology, 3, 1-5.

Wang, P., Hen, W. H., Zou H. (2004) Research on Agile Turn Reaction Jet Control of Air-to-air Missile. Journal of Beijing University of Aeronautics and Astronautics, 5, 95-399.

Taur, D. R., Chern, J. S. (1997) Optimal Thrust Vector Control of Tactical Missiles. AIAA Guidance, Navigation and Control Conference, 200-217.

Taur, D. R., Chern, J. S. (1999) An Optimal Composite Guidance Strategy for Dogfight Air-to-Air IR Missiles. AIAA Guidance, Navigation and Control Conference, 662-671.

Sim, Y. C., Leng, S. B. (2000) An All-Aspect Near-Optimal Guidance Law. Dynamics and Control, 10, 165-177.

Kim, K. U., Kang, S., Kim, H. J., Lee, C. H., Tahk, M. J. (2010) Realtime Agile-Turn Guidance and Control for an Air-to-Air Missile. AIAA Guidance, Navigation, and Control Conference, AIAA2010-7745.

Yuan, L. Y, Wu, J. F., Yu, L. Y., Cui, J. S., Sun, L. L. (2011) A Study of Chattering Suppression in Sliding Mode-Based Missile Guidance Law. Proceedings of the 6th International Forum on Strategic Technology, 924-926.

Mario, I., Ajay, T. (1993) Simultaneous Reaction Jet and Aerodynamic Control of Missile Systems. AIAA Guidance, Navigation and Control Conference, 347-354.

Li, B. G. (2012) Research on Key Technology of Compound Guidance for Short Range Air-to-air Missile. Electro Optics and Control, 9, 23-28.

Ma, K. M., Zhao, H., Zhang, D. C. (2011) Design and Realization of Compound Control of Direct Lateral Force and Aerodynamic Force for Missile. Journal of Astronautics, 2, 310-316.

Duan, D. D., Shen, X. L. (2012) Application and Analysis of Thrust Vector Technology in Air-to-air missile. Manoeuvrable Missile, 4, 2012, 84-87.

Mary Jane, G., Paul, W., Julius B. (2000) A Numerical Investigation of Supersonic Jet Interaction for Finned Bodies. 38th Aerospace Sciences Meeting and Exhibit.

Rex, C., Don, M., Anthony, D. (2000) CFD Analysis of Lateral Jet Interaction Phenomena for the THAAD Interceptor. 38th Aerospace Sciences Meeting and Exhibit.

Mavriplis, D. J. (1988) Accurate Multi-grid Solution of the Euler Equations on Unstructured and Adaptive Meshes. 1st National Fluid Dynamics Conference.

Oliveira, M., Lu, P., Liu, X., Liu, C. (2009) Universal High Order Subroutine with New Shock Detector for Shock Boundary Layer Interaction. 47th AIAA Aerospace Sciences Meeting Including the New Horizons Forum and Aerospace Exposition.

Islam, H., Rahaman, M., Islam, M. R., Akimoto, H. (2019) Application of a RaNS and PF-Based Method to Study the Resistance and Motion of a Bulk Carrier. Journal of Marine Science and Application, 3, 271-281.

Guo, M. L., Wang, Y. D., Tan, J. J., Ling, Q. G., Dai, J. (2019) Meshless Method Coupled with Different Reynolds Average Turbulence Model for Solving Navier-Stokes Equation. Journal of Nanjing University of Science and Technology, 5, 548-555.